Validation of GATE Monte Carlo simulations of the GE Advance/Discovery LS PET scanners

C. Ross Schmidtlein,[a] Assen S. Kirov, Sadek A. Nehmeh, Yusuf E. Erdi, John L. Humm, and Howard I. Amols
Department of Medical Physics, Memorial Sloan-Kettering Cancer Center, 1275 York Avenue, New York, New York 10021

Luc M. Bidaut[b]
Department of Imaging Physics, The University of Texas M.D. Anderson Cancer Center, 1515 Holcombe Blvd., Houston, Texas 77230-1439

Alex Ganin, Charles W. Stearns, and David L. McDaniel
GE Healthcare Technologies, 3000 N. Grandview Blvd., Waukesha, Wisconsin 53188

Klaus A. Hamacher
Weill Medical College of Cornell University, 525 East 68th Street, New York, New York 10021

(Received 17 February 2005; revised 29 August 2005; accepted for publication 1 September 2005; published 28 December 2005)

The recently developed GATE (GEANT4 application for tomographic emission) Monte Carlo package, designed to simulate positron emission tomography (PET) and single photon emission computed tomography (SPECT) scanners, provides the ability to model and account for the effects of photon noncollinearity, off-axis detector penetration, detector size and response, positron range, photon scatter, and patient motion on the resolution and quality of PET images. The objective of this study is to validate a model within GATE of the General Electric (GE) Advance/Discovery Light Speed (LS) PET scanner. Our three-dimensional PET simulation model of the scanner consists of 12 096 detectors grouped into blocks, which are grouped into modules as per the vendor's specifications. The GATE results are compared to experimental data obtained in accordance with the National Electrical Manufactures Association/Society of Nuclear Medicine (NEMA/SNM), NEMA NU 2-1994, and NEMA NU 2-2001 protocols. The respective phantoms are also accurately modeled thus allowing us to simulate the sensitivity, scatter fraction, count rate performance, and spatial resolution. In-house software was developed to produce and analyze sinograms from the simulated data. With our model of the GE Advance/Discovery LS PET scanner, the ratio of the sensitivities with sources radially offset 0 and 10 cm from the scanner's main axis are reproduced to within 1% of measurements. Similarly, the simulated scatter fraction for the NEMA NU 2-2001 phantom agrees to within less than 3% of measured values (the measured scatter fractions are 44.8% and 40.9±1.4% and the simulated scatter fraction is 43.5±0.3%). The simulated count rate curves were made to match the experimental curves by using deadtimes as fit parameters. This resulted in deadtime values of 625 and 332 ns at the Block and Coincidence levels, respectively. The experimental peak true count rate of 139.0 kcps and the peak activity concentration of 21.5 kBq/cc were matched by the simulated results to within 0.5% and 0.1% respectively. The simulated count rate curves also resulted in a peak NECR of 35.2 kcps at 10.8 kBq/cc compared to 37.6 kcps at 10.0 kBq/cc from averaged experimental values. The spatial resolution of the simulated scanner matched the experimental results to within 0.2 mm. [DOI: 10.1118/1.2089447]

I. INTRODUCTION

Positron emission tomography (PET) imaging, especially when combined with computed tomography (CT) as in PET/CT scanners, is rapidly becoming an essential adjuvant tool for defining the tumor target-volume in radiation therapy (RT).[1,2] However, the spatial resolution of PET is far poorer than that of CT or magnetic resonance imaging (MRI). Many factors including photon noncollinearity, off-axis detector penetration, detector size and response, positron range, photon scatter, and patient motion contribute to decreased PET resolution and image degradation.[3–6] Modern Monte Carlo tools can aid in assessing and overcoming these deficiencies. The purpose of this paper is to validate a Monte Carlo model for the simulation of the GE Advance/Discovery LS PET scanner in order to provide an accurate model for further research regarding the optimization of the performance of PET. Because the PET detectors and gantry electronics of the Advance and Discovery LS scanners are identical, and because the structure and end shielding are very similar, this simulation validation study covers both machines.

The GATE (GEANT4 application for tomographic emission) Monte Carlo package was developed by the OpenGATE collaboration.[7–10] It is an open-source extension of the GEANT4 Monte Carlo toolkit[11] and the ROOT object oriented

data analysis framework.[12] The use of GEANT4 as the basis of this package offers benefits that are described by Buvat and Castiglioni.[13] The most advantageous features are (1) GEANT4 is an open-source project with broad international support and (2) the underlying physics data and algorithms used by GEANT4 are well validated and constantly updated. Thus, as new features and refinements become available they are easily linked to GATE allowing it to continually expand and improve in order to meet rising technological demands and to incorporate new capabilities.[14]

The scanner's physical specifications were obtained from GE Healthcare and from direct measurements. The data collection system within GATE enables the modeling of the signal processing chain that is analogous to that of a real PET scanner.

For validation purposes the National Electrical Manufactures Association (NEMA) protocols[15–17] regarding sensitivity, scatter fraction, count rates, and spatial resolution were selected. These protocols collectively represent a series of reproducible experiments which characterize a scanner and which are well reported in the literature.

Several validation studies of GATE models for PET, SPECT, and small animal PET have recently been completed.[18] These include results for the ECAT EXACT HR+ PET scanner by Jan *et al.*[19] and for the Philips Allegro PET scanner by Lamare *et al.*[20] For SPECT, several commercial and prototype systems have been examined with detailed results of the Philips AXIS reported by Staelens *et al.*[21] and of the GE Discovery ST Xli by Assie *et al.*[22] In addition, the validation of several small animal PET scanners have been reported by Santin *et al.*,[14] by Jan *et al.*,[23] by Rey *et al.*,[24] by Lazaro *et al.*,[25] by Simon *et al.*,[26] and by Rannou *et al.*[27] A summary of the results from these studies is contained in the GATE release document by Jan *et al.*,[10] which also includes some preliminary results from this paper.[28]

As mentioned above, only two validation studies of large commercial PET scanners have been performed to date. This study represents the first validation of GATE for the GE Advance/Discovery LS PET scanner (DLS) and addresses the scanner's sensitivity, scatter fraction, resolution, and temporal curves. Detailed studies of the effects of a few selected scanner parameters (e.g., the couch, the dead time models, and the data analysis tools used on the results) are performed. In addition, the results from an analytical model for the single and random count rates are compared to GATE simulations. Finally, a description of the strategy for building sinograms from the simulated data using the geometry input system within GATE is presented in the appendix.

II. METHODS

In this section the model (i.e., the geometry, physics, and signal processing), the measurement protocols, and the count rate performance of the GATE coincidence modeling are described in detail.

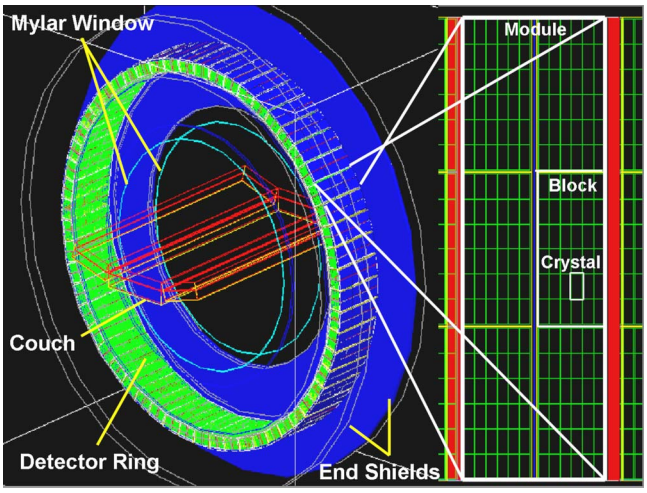

FIG. 1. GATE simulation model of the GE Advance/Discovery LS PET scanner. The proximal end shield, the couch, and the Mylar cover are depicted via wire-frame lines. In addition, an expanded view of the detector module, block, and crystal arrangement is shown.

A. Model description

1. Geometry

GATE uses combinations of simple shapes (e.g., boxes, spheres, and cylinders, as defined in GEANT4) to generate complex geometric structures. The software's limitations with regard to generating adequately complex shapes are well within the tolerance and design of these scanners. However, as a system's geometry grows more complex the simulation times can greatly increase since each boundary crossing by a particle is treated as a separate interaction. The model presented in this paper emphasizes geometric accuracy over computational cost. Every effort has been made to make this model as realistic as possible with respect to the geometry and physics of photon and charged particle transport.

The scanner, shielding, and phantoms were modeled as follows. In accordance with the real tomograph, the simulated GE Advance/Discovery LS PET scanner has 56 detector modules arranged in a ring. Each of these modules is comprised of six detector blocks (arranged in three blocks axially, by two blocks tangentially) which in turn contain 36

TABLE I. Default GEANT4 physics data libraries.

EPDL97[a] Evaluated photon data library	EEDL[b] Evaluated electron data library	EADL[c] Evaluated atom data library
Physics processes		
Compton scattering Pair production Photoelectric effect Rayleigh effect	Bremsstrahlung Ionization	Fluorescence Auger effect

[a]Reference 32.
[b]Reference 33.
[c]Reference 34.

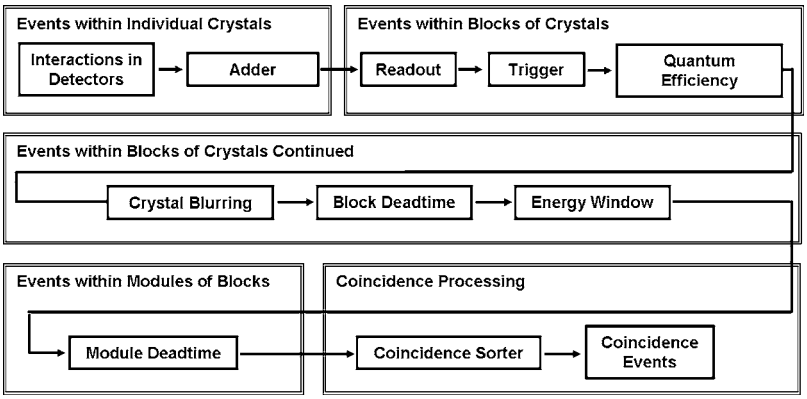

FIG. 2. Typical signal processing chain simulated by GATE used to convert the particle interactions within the detectors into coincidence counts.

Bismuth Germanium Oxyde (BGO) crystals each. This arrangement consists of 18 detection rings, each one with 672 crystals, for a grand total of 12 096 crystals. The dimensions of the individual crystals are approximately 4 mm $\times$ 8 mm $\times$ 30 mm.[29,30] In addition, the shielding and packing materials within the detector blocks, the shielding surrounding the scanner rings, and the couch are also accounted for in the model. The resultant digital model of the scanner is shown in Fig. 1. The phantoms are modeled separately using the dimensions and tolerances as described in the published NEMA standards. Additional details concerning the phantoms are given in Sec. II B.

2. Physics and Monte Carlo data

The GATE program is based upon the GEANT4 Monte Carlo simulation toolkit[11] which has been tested through direct comparison with experiments and other validated Monte Carlo codes as described in the GEANT4 release paper[11] and in Carrier *et al.*[31] The GEANT4 low energy models for photon interactions (Rayleigh, Photoelectric, and Compton) were used with the following energy and range cuts for photons and electrons; electron range=2 mm, δ ray=10 keV, and x-ray=10 keV. In these simulations the default GEANT4 libraries[32–34] (see Table I) and user-defined material data sets were used to match the material's compositions and densities as closely as possible to those of the scanner.

3. Signal processing

GATE also has the ability to convert photon interactions into counts in a manner analogous to that of a real scanner's detectors and electronics. This is accomplished in GATE by a series of signal processing routines known collectively as the *digitizer*. Each module of the *digitizer* mimics a separate portion of a scanner's signal processing chain. (For a full description of the *digitizer* features available within GATE see the *GATE Users Guide*.[35])

A sequence of digitizer modules to simulate the complete signal processing chain (Fig. 2) was used in the simulation. This sequence begins with the *Adder* module which integrates the energy deposition of a particle interacting within a single crystal. Next, the *Readout* module integrates the results from the *Adder* module within a block of crystals to create a pulse. Following this, a 100 keV detector threshold is applied to the signal to model this aspect of the scanner. Then a *Blurring* module applies a detection efficiency factor and a Gaussian energy blur [full width at half-maximum (FWHM) of 20% referenced at 511 keV] to the integrated interactions within the detector blocks. Next, a *Deadtime* module is inserted to create deadtime at the Block level that is triggered by the pulses within a block. Following this, another deadtime module is applied at the Module level of the scanner to account for the multiplexor processing of the single events. An energy-window discriminator is then applied via the *Thresholder* and *Upholder* modules (either 300 to 650 keV or 375 to 650 keV). Finally, the remaining pulses are sorted by the *Coincidence* module (6.25 ns window). External to GATE, a correction is applied to the random counts and an additional deadtime is applied to the coincidence data via post processing.

In the GATE version (1.2.0) used in this study, the coincidence processing within GATE rejects multiple coincidences, while the GE PET scanner does not. The random count rate is corrected to account for this loss of counts as described at the end of Sec. II C.

It has been shown by Erikkson *et al.*[36] that two paralyzable deadtimes (one at singles level and one at the coincidence level) are sufficient to model the count rate performance of a PET scanner. Employing a similar model, we determined both the Block and Coincidence level deadtimes by a least-squares iterative process. In this way, we obtained a 625 ns deadtime for the singles at the Block level followed by a 332 ns deadtime for the coincidence count rate.

The sensitivity, scatter fraction, and spatial resolution

TABLE II. NEMA Protocols used in this study.

NEMA NU2-2001[a]	NEMA NU2-1994[b]	NEMA/SNM[c] recommendations
Sensitivity Scatter fraction Count rates Spatial resolution	Scatter fraction	Scatter fraction

[a]Reference 17.
[b]Reference 16.
[c]Reference 15.

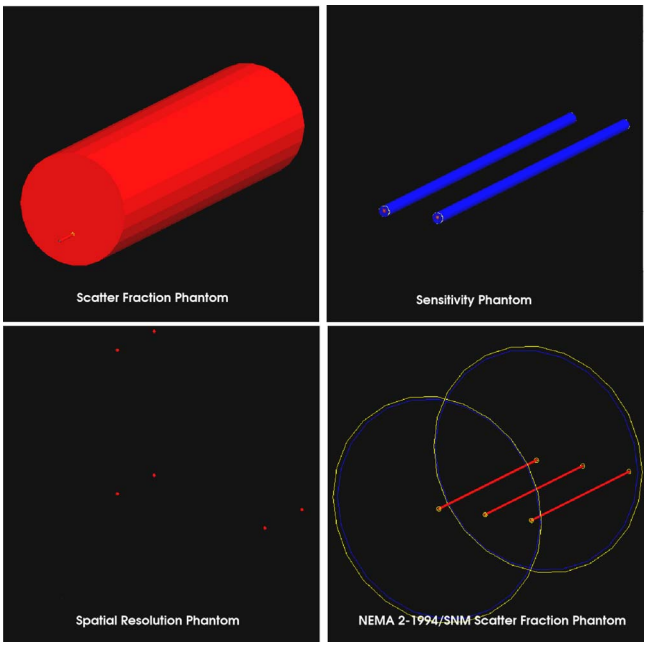

FIG. 3. Virtual NEMA phantoms used in the simulation. From left to right and top to bottom: NEMA NU2-2001[17] scatter fraction, sensitivity, spatial resolution, and the NEMA 1994/SNM[16,15] scatter fraction phantoms.

simulations were performed at low activities as directed by NEMA in order to keep the results independent of deadtime and random coincidences.

4. Coincidence processing

The coincidence pairs produced by GATE required additional sorting into sinograms and Michelograms for use in a portion of the scatter faction analysis and in the image reconstruction. The strategy used to map the coincidences to lines of response (LOR's), and LOR's to sinograms is described in the Appendix.

B. Evaluation protocols

The NEMA protocols represent a baseline for assessing and comparing the fundamental characteristics of a PET scanner.[15–17] The tests described in these protocols measure a scanner's spatial resolution, scatter fraction, count losses, randoms, sensitivity, accuracy, and image quality. The results of these tests are well documented and are available for most commercial PET scanners, including the GE Advance/Discovery LS PET scanner. For these reasons, the NEMA protocols (with an emphasis on NU2-2001) were chosen as the basis for validating GATE simulations. Only the sensitivity, scatter fraction, count rates, and spatial resolution tests were examined. From these, only the spatial resolution test requires image reconstruction, which is imposed as filtered back projection (FBP) with a ramp filter, thus making it generic. These tests are listed in Table II. The simulated NEMA phantoms are shown in Fig. 3.

C. Analytical single and random count rate model

In addition to an experiment, one can evaluate the signal processing capabilities of GATE by comparing the simulation model of a PET scanner to an analytic model. The count rates can be estimated by a simple analytical model for a circularly symmetric scanner and source similar to the one presented by Hoffman *et al.*[37]

In principle, if energy cuts are ignored, the number of singles can be estimated by an analysis based upon the source activity and the scanner geometry. If the NEMA NU2-2001 scatter fraction analysis is performed using a cylindrical symmetric source centered in the scanner, then the singles can be estimated by an equation of the form

$$S_0 = 2AF_{1\to 2}C_{\text{geom}}B_{\text{up}}\exp(-\mu_{\text{ph}}x_{\text{ph}}) \times[1-\exp(-\mu_{\text{BGO}}x_{\text{BGO}})], \quad (1)$$

where A is the activity of the phantom, $F_{1\to 2}$ is the geometric view factor[38] from the activity source to the scanner's rings, C_{geom} is a geometric correction to account for non-detector materials in the rings, $\exp(-\mu_{\text{ph}}x_{\text{ph}})$ is the attenuation due to the phantom of radius x_{ph} and an attenuation coefficient of μ_{ph}, with a build-up factor B_{up} to account for photons scattered into the field of view, and $[1-\exp(-\mu_{\text{BGO}}x_{\text{BGO}})]$ to account for the number of photons stopped by the detectors made up of BGO crystals each having a thickness of x_{BGO} and an attenuation coefficient of μ_{BGO}.

In a manner similar to that proposed by Hoffman *et al.*[37] and used by Santin *et al.*[14] and Simon *et al.*[26] the random counts can be estimated from the observed single count rates. This is shown by the equation

$$R_0 = 2\tau\frac{C_{\text{LOR}}}{[(NR)^2-NR]/2}S_0^2, \quad (2)$$

where τ is the coincidence time window, N is the number of detectors per ring, and R is the number of rings. The term C_{LOR} accounts for the number of LOR's defined by GATE and is given by

$$C_{\text{LOR}} = an_r n_\phi R^2, \quad (3)$$

where n_r and n_ϕ are the number of radial and tangential sinogram bins and $a=0.64$ is a fit parameter that accounts for coincidences not allowed by GATE. This parametrization is justified because the goal of this model is to verify the reproducibility of the randoms' trend as a function of activity. The GATE version (1.2.0) used in this study rejects multiple coincidences. As a result, the random rates must be corrected by using a paralyzable deadtime of 2τ.[39] This results in the equation

$$R_0 = 2\tau\frac{C_{\text{LOR}}}{[(NR)^2-NR]/2}S_0^2e^{-2\tau S_0}. \quad (4)$$

Both the single and random count rates can further be corrected for distinct deadtimes that may exist on block, and module subsets of the scanner's geometry. This is done by applying paralyzable deadtimes to Eqs. (1) and (4). If the deadtime at the Block level is DT_1, then this results in

TABLE III. Comparison of 3D sensitivity measurements between the GE Advance/Discovery LS scanner and the GATE simulation with and without efficiency corrections.

Radial position (cm)	Published data (cps/kBq)	GATE w/o eff. corrections (cps/kBq)	GATE w/eff. corrections (cps/kBq)
$R_0=0$	6.41±0.16[a]	8.14±0.02	6.44±0.01
$R_{10}=10$	6.56±0.32[a]	8.31±0.02	6.53±0.01
Ratio (R_0/R_{10})	0.977	0.980	0.986

[a]Reference 41.

$$S_1 = S_0 e^{-DT_1 S_0/(N_{\text{Blocks}})}, \tag{5}$$

and

$$R_1 = 2\tau \frac{C_{\text{LOR}}}{[(NR)^2 - NR]/2} S_1^2 e^{-2\tau S_1} \tag{6}$$

for singles and randoms, respectively, where N_{Blocks} is the number of blocks in the scanner, 336. Likewise, for an additional deadtime of DT_2 at the Module level the equations are

$$S_2 = S_1 e^{-DT_2 S_1/(N_{\text{Modules}})}, \tag{7}$$

and,

$$R_2 = 2\tau \frac{C_{\text{LOR}}}{[(NR)^2 - NR]/2} S_2^2 e^{-2\tau S_2} \tag{8}$$

for singles and randoms, respectively, where N_{Modules} (=56) is the number of modules in the scanner.

The simplified model given above is useful in verifying the deadtime and coincidence sorting behavior of the GATE digitizer. However, because energy window cuts are not included the rates described by these equations do not fully reflect the actual performance of a real-life PET scanner.

Based upon the above discussion a correction to the random count rate to account for GATE's rejection of multiple coincidences can be derived from Eq. (4):

$$R_{\text{GATE}}^{\text{Corr}} = R_{\text{GATE}} e^{2\tau S_2}. \tag{9}$$

This correction is applied to the GATE simulated randoms for the time curve results presented in Sec. III C 1.

III. RESULTS

The results are compared to published data from Lewellen *et al.*,[30] Daube-Witherspoon *et al.*,[40] Kohlmyer *et al.*,[41] and commissioning data performed at New York Hospital with a GE Discovery LS (NYH DLS).

A. Sensitivity

A comparison of the sensitivity of the GATE simulation to experimental values is presented in Table III. The third column contains GATE data without efficiency corrections. The fourth column lists the results when a 90.58% quantum efficiency (QE) is applied to individual events within the blocks in the *digitizer*. This efficiency was varied as a free parameter until the best agreement with experimental results was obtained. In addition to correcting for the detector QE in our model, this parameter partially accounts for intrinsic modeling approximations in the scanner geometry and the signal processing chain.

B. Scatter fraction

A comparison of the scatter fraction results of the GATE simulations to those of the measured data is presented in Table IV. This table shows that the simulation's scatter fractions are very close to the measured values (within 1% to 5%). The computed scatter fraction differed by ~4% with the inclusion of the couch in the simulation. The difference between the two experimental data points for the 375 to 650 keV energy window is also about 4%. This result is also similar to that reported by Badawi *et al.*[42] (NEMA NU2-1994, 23.7% simulated to 28.0% measured), however the patient couch was not included. In addition, the scatter fraction calculations as determined by the NEMA analysis and by direct binning of the Monte Carlo data are compared in Fig. 4. As is shown in the figure, both methods are within 1% provided that enough coincidence events are counted (~20 k counts for these scanners). This result is similar to that seen by Badawi *et al.*[42] with SimSET,[43] a well-developed public domain Monte Carlo simulation package for emission tomography.

TABLE IV. Comparison of scatter fractions for the NEMA/SNM, NEMA NU2-1994, and NEMA NU2-2001 protocols.

Scatter fraction protocol	Energy window (keV)	Scanner data	GATE results	Couch
NEMA/SNM	300–650	36.0%[a]	35.9±0.1%	yes
NEMA 2-1994	300–650	34.7%[b]	36.0±0.1%	yes
NEMA 2-2001	300–650		48.1±0.3%	no
NEMA 2-2001	300–650	47.1%[b]	52.3±0.3%	yes
NEMA 2-2001	375–650		40.8±0.3%	no
NEMA 2-2001	375–650	44.8%(NYH)	43.5±0.3%	yes
NEMA 2-2001	375–650	40.9±1.4%[c]		yes

[a]Reference 30.
[b]Reference 40.
[c]Reference 41.

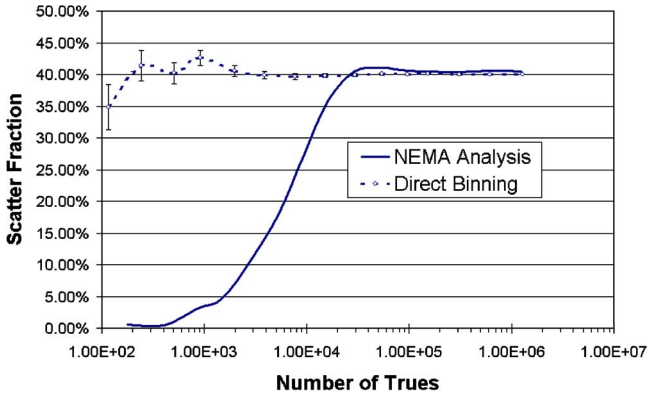

FIG. 4. Comparison of the scatter fraction values from the NEMA analysis to those determined from direct binning of the Monte Carlo data for a simulation without the couch.

C. Count rate performance

1. Comparison to experimental data

The count rate performance for trues, scatters, randoms, and noise equivalent counts without randoms subtraction are shown in Fig. 5. The noise equivalent count rate without randoms subtraction is calculated via

$$NECR_{1R} = \frac{T^2}{T+S+R}, \tag{10}$$

where T, S, and R are the true, scatter, and random count rates, respectively. The simulated peak true count rate is 139.2 kcps occurring at 21.6 kBq/cc and the simulated peak $NECR_{1R}$ is 35.2 kcps at 10.8 kBq/cc. In this figure, the random count rates are corrected for multiples as described by Eq. (9). Two paralyzable deadtimes are used as suggested by Eriksson *et al.*[36] The couch was included with the scatter fraction phantom in these simulations. In this figure the simulated count rates are compared to data from studies by Kohlmyer *et al.*[41] and our data from the NYH DLS.

2. Comparison to model

In Fig. 6, the predicted single rates are estimated from Eqs. (1), (5), and (7) and are compared to the values extracted from GATE. These figures are based upon models of the NEMA NU2-2001 scatter fraction phantom with a cylindrically symmetric source. The simulated single rates are in excellent agreement with the analytical model's values until the activity density reaches approximately 300 kBq/cc (6.5 GBq of total activity, not shown) at which point the predicted single rates fall off faster than the GATE single rates if a deadtime is applied. However, without an applied deadtime the single rates are within 0.5% of the estimated rates throughout the entire range. The predicted random count rates are compared to the results from GATE in Fig. 7. The general shapes of the curves are similar to one another until an activity concentration greater than 150 kBq/cc is reached (not shown), at which point the R_1 and R_2 randoms predicted by the model fall away faster than those calculated from GATE.

D. Spatial resolution

The images for the quantification of the spatial resolution were reconstructed using the Software for Tomographic Image Reconstruction (STIR) FBP3DRP code[44] without normalization correction.[46] In Table V the spatial resolution obtained from the simulations are compared to the experimental values obtained from the New York Hospital Discovery LS scanner data. Two sets of simulations were run to quantify the sensitivity of the scanner's resolution to the axial position of the source. In the first simulation, the sources were axially centered with respect to the crystals, whereas in the second simulation the sources were centered with respect to the axial gaps between the crystal rings. In addition, the lines of response were blurred via a Gaussian function with a FWHM of 4.75 mm to account for the light shielding both within and between the detector blocks, the inherent limitations of the resolution of the photomultiplier tube's (PMT) and the light scatter within the crystals. The results of the blurred LOR's are also presented in Table V.

IV. DISCUSSION

A. Sensitivity

The intrinsic sensitivity of the GATE simulation, shown in Table III, Column 3, is greater than that of the actual GE Advance/Discovery LS scanner by more than 20%. Several different factors may account for this behavior. Phenomena within a real detector-signal processing chain, not explicitly modeled in the simulation, includes block nonuniform energy resolutions, light spread and leakage, and PMT and optical coupling efficiencies. In addition, our GATE model of the GE Advance/Discovery LS PET scanner is an approximation and is based upon limited geometric information. Nevertheless, the simulated sensitivity variation as a function of the radius matches very well with the measured data (i.e., S_0/S_{10} is within 1% of measurements as seen in Table III) without applying any corrections. The correction of the sensitivity by the addition of an efficiency factor as a free parameter at the crystal level allowed the simulation to match the efficiency of the measured data without affecting the ac-

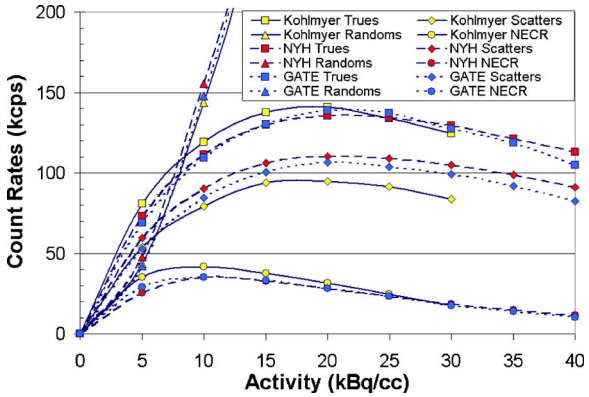

FIG. 5. 3D mode count rate response showing both simulated (GATE, dotted lines) and experimental data (Kohlmyer *et al.*,[41] solid lines, and NYH DLS, dashed lines).

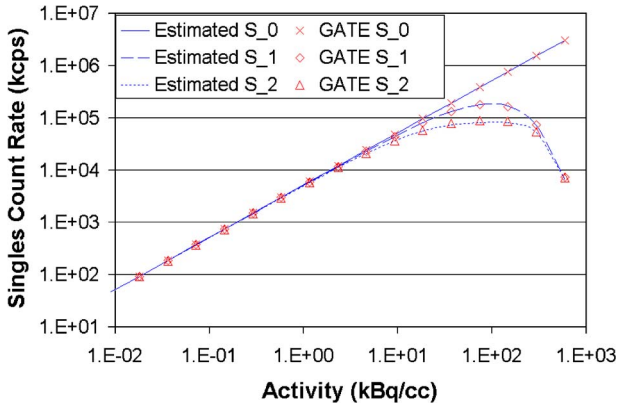

FIG. 6. Comparison of the estimated single count rates calculated from Eqs. (1), (5), and (7) (lines) to those produced by GATE (symbols) as a function of activity. In this figure, S_0 represents the single rate with no deadtime. S_1, and S_2 are the single rates with successive deadtimes applied to the Block and Module subsets of the scanner's geometry, respectively. No energy window cuts are used in these simulations.

curacy of either the radial sensitivity ratio or the scatter fraction. The addition of this efficiency factor (90.58%) is an important step for accurately modeling the count rate performance of the scanner because deadtime is quite sensitive to the detection rates of the crystals.

B. Scatter fraction

Both the direct binning of simulated events and the NEMA method were used to determine the random, true, and scatter coincidences from the Monte Carlo data. The results of these two methods agreed to within less than 1% at sufficient statistics, which is consistent with Badawi *et al.*[42] This result is shown in Fig. 4 and offers assurance that the NEMA approach is an accurate indication of the scatter fraction. However, the figure also indicates that at low counts the NEMA methodology is not only imprecise but inaccurate as well. Measurements where less than 5–6 counts per projection plane in the sinograms are gathered will result, due to a systematic error, in a smaller scatter fraction than the correct value. This problem occurs during the search for the maximum count for each projection plane. Due to the discreet nature of the data in the sinograms and the very large number of LOR's in a three-dimensional (3D) data set, a data set with too few counts can falsely identify scattered counts within the central maximum resulting in too many scattered counts being counted as true. Hence, the NEMA method does not strictly follow Poisson statistics when the number of counts is below a critical threshold. On the other hand, the count rate uncertainties in a GATE simulation do follow Poisson statistics. This is important because with NEMA NU 2-2001 scatter fraction phantom the coincidence event rate is currently on the order of $\sim 1-2$ events per second on a Pentium 4 2400 MHz computer depending upon the level of detail used in modeling the particle interactions.

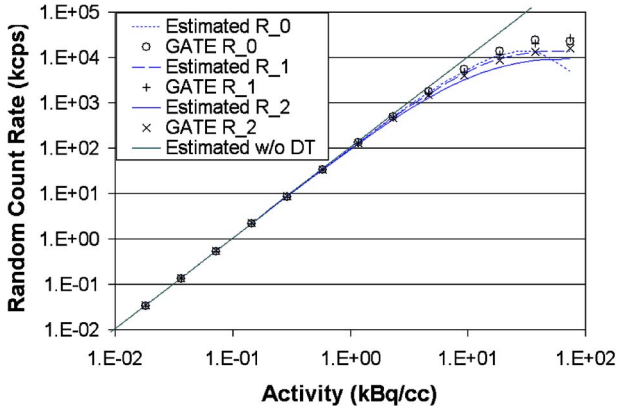

FIG. 7. Comparison of the predicted random count rates calculated from Eqs. (4), (6), and (8) (lines) to those produced by GATE (symbols) as a function of activity. In this figure, R_0 represents the random rates with no deadtime. R_1 and R_2 are the random rates with successive deadtimes applied to the Block and Module subsets of the scanner's geometry, respectively. No energy window cuts are used in these simulations.

C. Count rate performance

1. Comparison of Monte Carlo to experimental data

In order to mimic the behavior of a real PET scanner, a multiparametric search had to be performed in order to achieve a good fit with the measured count rate data. The relative performances of three different signal processor designs were examined: no deadtimes, deadtime on singles, and deadtimes on both singles and coincidence events. In each case it was necessary to correct the GATE simulation's random count rates using Eq. (9) to account for the loss of multiple coincidences in the simulations. For the case of no deadtimes the resulting data closely correlates with the low activity portions (<5 kBq/cc) of the curve, but at higher activities all count rates grow rapidly relative to the measured data. Using a deadtime only on singles resulted in good true, scatter, and random count rates, but the deadtime had to be varied with the count rate to accurately model the scanner's behavior above 10 kBq/cc. The simplest combination of deadtimes that resulted in a small least-squares error occurred when using a fixed paralyzable deadtimes at both the block and coincidence levels.

The results obtained with a constant block and coincidence deadtime model are shown in Fig. 5. This model predicts peak true count rates of 139.2 kcps at 21.6 kBq/cc compared to Kohlmyer *et al.*[41] with 141.2 kcps at 19.7 kBq/cc and to the NYH DLS data with 136.8 kcps at 23.3 kBq/cc. Thus, the simulated peak trues match those given by the averaged experimental data to within 0.5% and 0.1%, respectively. In addition, the simulation predicts a peak NECR of 35.2 kcps at 10.8 kBq/cc compared to Ref. 41 with 39.4 kcps at 9.3 kBq/cc and to the NYH DLS with 35.7 kcps at 10.6 kBq/cc. This results in larger relative errors for NECR's peak values and peak position than for that of the true count rates. The relative errors are 8.5% for the peak NECR's location and 6.3% for the peak's corresponding activity concentration when compared to the average experimental values.

TABLE V. 3D spatial resolution measurements of the GE Discovery LS PET scanner performed at New York Hospital compared to the results of a GATE simulation reconstructed with STIR without and with spatial crystal blurring.

Source position measured radially from the central axis		New York Hospital DLS 3D measurement (mm)	GATE 3D simulated crystal-centered (mm)	GATE 3D simulated gap-centered (mm)	GATE 3D with blurring crystal-centered (mm)	GATE 3D with blurring gap-centered (mm)
1 cm	Transaxial FWHM	5.1	3.9	3.9	5.0	5.0
	Axial FWHM	7.2	8.6	6.7	9.4	7.4
10 cm	Radial FWHM	5.5	4.4	4.4	5.4	5.4
	Tangential FWHM	4.9	4.0	4.0	5.1	5.1
	Axial FWHM	7.7	9.6	7.4	10.3	7.8

2. Comparison of Monte Carlo to the analytical model

In addition to comparing the count rate curves of the GATE simulations to published results, we also compared them to an analytical model. This allowed us to assess how well GATE collects single events and processes them into random coincidences. The results of these comparisons are shown in Figs. 6 and 7.

In previous studies by Santin *et al.*[14] and Simon *et al.*[26] the random rates based upon the single rates were examined for a geometry consisting of a source centered between two detectors. The source consisted of two independent particle sources each with a total activity of 10 MBq.

To compare the simplified geometry of these studies[14,26] to the model described in this paper, their results need to be related by a scaling factor for both singles and randoms. For the single count rates, this factor is given as a ratio of the source to detector view factors and for this study corresponds to approximately 1. For the case of the random count rate, this scaling factor depends upon both the coincidence window and the square of the single count rates, and is thus a product of the square of the ratio of the view factors and of the ratio of the coincidence windows that results in a factor of about 3. Therefore, the 10 MBq point source for single counts in Santin *et al.*[14] and Simon *et al.*[26] is equivalent to an activity concentration of 0.45 kBq/cc in the line source phantom for this study. For random counts, this is equivalent to an activity concentration of 1.4 kBq/cc.

Santin *et al.*,[14] and Simon *et al.*,[26] showed that GATE's prediction of random coincidences agreed well with a simple model over a range of activities when multiple coincidences were rejected. The results presented in this study support this conclusion by showing a similar agreement at equivalent activity densities. In addition, the current results show that deadtime effects in GATE are consistent with theoretical values over a much larger range than previously reported. Finally, we note that starting at very large activity concentrations the single event rates with the various deadtimes applied diverge from the predicted results. This divergence occurs near saturation activity concentrations greater than ~300 kBq/cc (where deadtime approaches 100%). This behavior may indicate the presence of floating-point truncation of the timing variable within GATE or GEANT4. However, measurements at such high activities (ten times greater than those reported in the literature[41]) are not currently relevant in nuclear medicine applications.

Similar behavior is seen in the random count rates' results. At very high activities the estimated random counts rates also fall away faster than those calculated by GATE. This occurs at activity concentrations greater than ~150 kBq/cc and may be due to GATE's coincidence restrictions that ignore LOR from singles that are within adjacent modules of one another and thus reduces the effect of deadtime from these singles. The divergence seen in the single rates at activity concentrations greater than ~300 kBq/cc is also seen in the randoms.

D. Spatial resolution

Without normalization corrections, as is shown in Table V, the maximum axial resolution is achieved when the source is placed between the crystals in the axial direction, while the resolution in the transverse direction remains largely the same regardless of the axial position of the source. In fact GATE simulation shows that the resolution in the gap-centered source location is ~24% better than if the source is axially centered with the faces of the detectors. The table shows that the simulated scanner's spatial resolution without blurring is better than that of the actual PET scanner. This is to be expected: The spatial blurring that takes place on a real scanner due to crosstalk between the crystals and the loss of resolution due to the Anger logic of the PMT's is not directly accounted for in the current simulations. This effect is mimicked by applying a Gaussian blur on the sinograms produced by GATE. The agreement between the blurred simulated images and those obtained at New York Hospital for the GE Discovery LS are within 0.2 mm (~5%), however differences of up to 2.5 mm are seen if the sources are not placed properly with respect to the axial direction. As pointed out above, the results presented here are without normalization corrections. It is anticipated that normalization corrections will reduce the axial blurring inhomogeneity seen in this study. In addition, normalization corrections may cause the spatial blurring kernel to change. A description of a normalization correction scheme and its effect on the resolution will be addressed in the future.

V. CONCLUSIONS

The results of this study indicate that GATE can accurately simulate the main performance characteristics of the GE Advance/Discovery LS PET scanner. Using GATE's *digitizer* and by adhering to NEMA protocols, the sensitivity, scatter fraction, count rates, and spatial resolution can be accurately simulated. The validation of a GATE model for the GE Advance/Discovery LS PET scanner represents an important first step in performing simulation studies for further understanding the performance of this and other similar PET scanners and also for improving and expanding their clinical utility. In future studies, the information gleaned from Monte Carlo simulations will aid in further improvement of the quality, accuracy, and usefulness of PET images.

ACKNOWLEDGMENTS

The authors want to thank Dr. Clifton Ling from the Department of Medical Physics, and Dr. Steven Larson from the Department of Radiology at Memorial Sloan-Kettering Cancer Center for their support of this work. In addition, the authors would like to acknowledge Brad Beattie from the Department of Neurology for many fruitful discussions regarding PET signal processing. Also, the authors are indebted to Dr. Sebastien Jan and Dr. Christian Morel for all of the help and the insight given by the OpenGATE collaboration. Finally, they would like to thank Dr. Tin-Su Pan of MD Anderson Cancer Center for his assistance with image reconstruction. This study was funded in part by a seed grant from the Department of Medical Physics at Memorial Sloan-Kettering Cancer Center and by the U.S. National Cancer Institute Grant No. CA059017-12.

APPENDIX: DATA PROCESSING

In order to perform certain aspects of the NEMA analysis we utilized a sinogram binning methodology that merits discussion. It represents a strategy for converting simulated coincidence pairs (LOR's) into sinograms that is of general interest and can be potentially useful for PET scanner data analysis that relies either upon sinograms or on reconstructed images. The LOR binning strategy employed here is more general than the one shown graphically by Hoffman *et al.*[45]

1. Rebinning GATE coincidences

GATE uses the Crystal, Block, and Module identification numbers to organize detection events into sinograms. This nomenclature is comparable to that used in actual scanners. In this scanner, the events are identified and stored by subdividing the scanner into 36 Crystals per Block, 6 Blocks per Module (in a two by three Block configuration), and 56 Modules for the complete gantry.

In this case, the GATE crystal, block, and module ID's for each coincidence pair are converted into crystal-ring pairs via the following equations: (INT and MOD functions take the integer and modulus of their arguments, respectively)

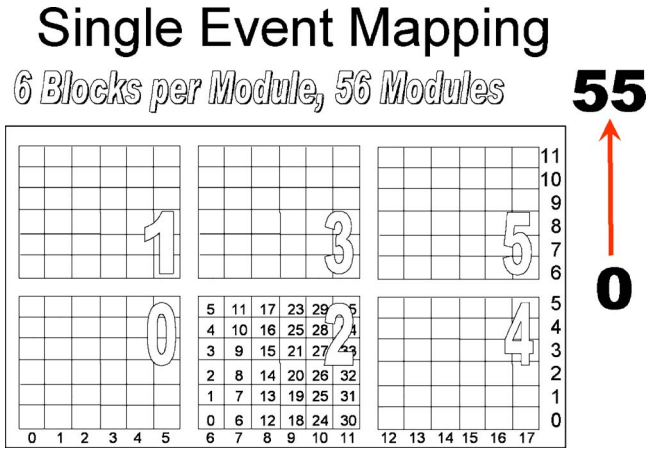

FIG. 8. Indexing scheme used by GATE to define detector locations within a Module. Note that the scanner has 56 Modules, each containing 6 blocks, which in turn contain 36 crystals each.

$$\mathrm{Ring}_{1,2} = \mathrm{INT}\left(\frac{\mathrm{CrystalID}_{1,2}}{6}\right) + 6 \times \mathrm{INT}\left(\frac{\mathrm{BlockID}_{1,2}}{2}\right), \tag{A1}$$

and

$$\mathrm{Crystal}_{1,2} = \mathrm{MOD}(\mathrm{CrystalID}_{1,2},6) + 6 \times [\mathrm{MOD}(\mathrm{BlockID}_{1,2},2) + 2 \times \mathrm{ModuleID}_{1,2}]. \tag{A2}$$

The subscripts 1,2 correspond to each of the detected events that make up the coincidence pair. This indexing used by GATE is shown in Fig. 8.

2. Building sinograms

The crystal-ring pairs represent lines of response (LOR) that are rearranged (binned) into a Michelogram format (developed by Christian Michel[46]). In this format, the LOR's are binned into a block matrix with index dimensions in the ϕ (azimuthal), r (radial), and θ (ring difference) directions.

The azimuthal binning of the LOR's is achieved by noting that for each projection plane the sum of the crystal numbers (C#) for a coincidence pair will always sum to one of two numbers that are unique to a particular projection plane. These two numbers are offset from one another by the total number of crystals in the scanner's ring (i.e., in the GE Advance/Discovery LS scanner $N=672$, thus sum=C# and C#+672). The index i for a given ϕ can then be expressed as

$$i = [(\mathrm{Crystal}_1 + \mathrm{Crystal}_2) + \mathrm{Const.}], \tag{A3}$$

where the Const. is an arbitrary offset which satisfies the boundary condition $\phi=0$. In the case of interlacing, $i \in [0, N/2)$, and ϕ_i is therefore given by

$$\phi_i = \frac{2\pi i}{N}. \tag{A4}$$

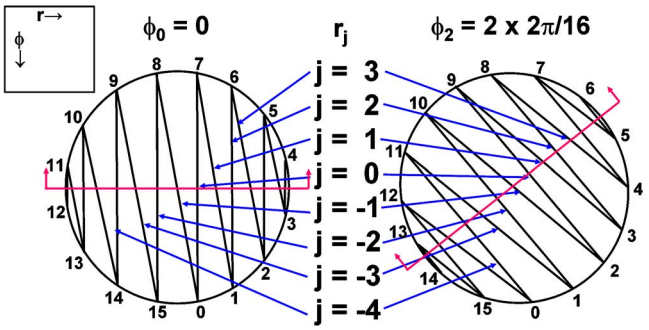

FIG. 9. Simple example that shows the sinogram indexing for two projection planes of a scanner with 16 detectors that interlaces with ϕ into r.

Radial binning is done by observing that the radial distance from the center of the scanner is related to the index difference of the crystals in the pair. In terms of indexing, the index j for r can be expressed as

$$|j| = N/2 - |\text{Crystal}_1 - \text{Crystal}_2|, \tag{A5}$$

with $j \in [0, N/2)$ for the case of interlacing. The sign of j is determined by the position of the LOR relative to ϕ_i

$$j = \begin{cases} +|j| & \text{if crystal}_{1,2} \in [i, i+N/2] \\ -|j| & \text{otherwise} \end{cases}. \tag{A6}$$

Another way of stating this is that a LOR for a crystal pair in the right-half plane, with respect to the LOR's projection plane, will have a positive index, whereas the left-half plane will have a negative index. Thus for a scanner of radius R, this results in the radial distance r_j being expressed by

$$r_j = R \sin\left[\pi\left(\frac{j+1/2}{N}\right)\right]. \tag{A7}$$

Lastly, the ring difference, or the index of the axial angle θ, is simply given by the ring difference as determined above in Eq. (A2). Here coincidence pairs with $\theta > 0$ are stored as $(\text{ring}_1, \text{ring}_2)$ while those with $\theta < 0$ are stored as $(\text{ring}_2, \text{ring}_1)$. They are assigned in the following manner:

$$(\text{ring}_1, \text{ring}_2) \; \forall \; \text{crystal}_1 \in [i - N/4, i + N/4], \tag{A8}$$

and

$$(\text{ring}_2, \text{ring}_1) \; \forall \; \text{crystal}_2 \in [i - N/4, i + N/4]. \tag{A9}$$

The crystal that lies in the lower-half plane with respect to the ith projection plane will define the first index.

In practice, the coincidence events described in this section are interlaced from ϕ into r. This has the effect of halving the number of ϕ indices and doubling the number of r indices; $i \in [0, N) \rightarrow [0, N/2)$, and $j \in [0, N/4) \rightarrow [0, N/2)$. Figure 9 illustrates the indexing strategy used to convert the detector and ring number pairs into sinogram counts.

[a]Electronic mail: schmidtr@mskcc.org
[b]Previously at Department of Radiology, Memorial Sloan-Kettering Cancer Center, 1275 York Avenue, New York, New York 10021.

[1]C. C. Ling, J. L. Humm, S. M. Larson, H. I. Amols, Z. Fuks, S. Leibel, and J. A. Koutcher, "Toward multidimensional radiotherapy (MD-CRT): Biological imaging and biological conformality," Int. J. Radiat. Oncol., Biol., Phys. **47**, 551–560 (2000).
[2]E. Pelosi, C. Messa, S. Sironi, M. Picchio, C. Landoni, V. Bettinardi, L. Gianolli, A. Del Maschio, M. C. Gilardi, and F. Fazio, "Value of integrated PET/CT for lesion localization in cancer patients: A comparative study," Eur. J. Nucl. Med. Mol. Imaging **31**(7), 932–939 (2004).
[3]V. I. Goldanskii, "Physical chemistry of the positron and positronium," At. Energy Rev. **6**, 3–148 (1968).
[4]M. Phelps, E. J. Hoffman, S. Huang, and M. M. Ter-Pogossian, "Effect of positron range on spatial resolution," J. Nucl. Med. **16**, 649–652 (1975).
[5]S. E. Derenzo, "Precision measurements of annihilation point spread distribution for medically important positron emitters," *Proc. of the 5th International Conference on Positron Annihilation* (Japan Institute of metals, Sendai, Japan, 1979), pp. 819–823.
[6]D. W. Rickey, R. Gordon, and W. Huda, "On lifting the inherent limitations of positron emission tomography by using magnetic fields (Mag-PET)," Automatica **14**, 355–369 (1992).
[7]D. Strul, "Preliminary specifications of a Geant4-based framework for nuclear medicine simulations," *ClearPET Technical Report* (University of Lausanne, Switzerland, 2001).
[8]D. Strul, "Specification of a Geant4-based nuclear medicine simulation framework," *ClearPET Technical Report* (University of Lausanne, Switzerland, 2001).
[9]D. Strul, G. Santin, D. Lazaro, V. Breton, and C. Morel, "GATE(Geant4 application for tomographic emission): A PET/SPECT general purpose simulation platform," Nucl. Phys. B **125**, 75–79 (2003).
[10]S. Jan, G. Santin, D. Strul, S. Staelens, K. Assié, D. Autret, S. Avner, R. Barbier, M. Bardiès, P. M. Bloomfield, D. Brasse, V. Breton, P. Bruyndonckx, I. Buvat, A. F. Chatziioannou, Y. Choi, Y. H. Chung, C. Comtat, D. Donnarieix, L. Ferrer, S. J. Glick, C. J. Groiselle, D. Guez, P.-F. Honore, S. Kerhoas-Cavata, A. S. Kirov, V. Kohli, M. Koole, M. Krieguer, D. J. van der Laan, F. Lamare, G. Largeron, C. Lartizien, D. Lazaro, M. C. Maas, L. Maigne, F. Mayet, F. Melot, C. Merheb, E. Pennacchio, J. Perez, U. Pietrzyk, F. R. Rannou, M. Rey, D. R. Schaart, C. R. Schmidtlein, L. Simon, T. Y. Song, J.-M. Vieira, D. Visvikis, R. Van de Walle, E. Wieers, and C. Morel, "GATE: A simulation toolkit for PET and SPECT," Phys. Med. Biol. **49**, 4543–4561 (2004).
[11]S. Agostinelli, J. Allison, K. Amako, J. Apostolakis, H. Araujo, P. Arce, M. Asai, D. Axen, S. Banerjee, G. Barrand, F. Behner, L. Bellagamba, J. Boudreau, L. Broglia, A. Brunengo, H. Burkhardt, S. Chauvie, J. Chuma, R. Chytracek, G. Cooperman, G. Cosmo, P. Degtyarenko, A. Dell'Acqua, G. Depaola, D. Dietrich, R. Enami, A. Feliciello, C. Ferguson, H. Fesefeldt, G. Folger, F. Foppiano, A. Forti, S. Garelli, S. Giani, R. Giannitrapani, D. Gibin, J. J. Gmez Cadenas, I. GonzAlez, G. Gracia Abril, G. Greeniaus, W. Greiner, V. Grichine, A. Grossheim, S. Guatelli, P. Gumplinger, R. Hamatsu, K. Hashimoto, H. Hasui, A. Heikkinen, A. Howard, V. Ivanchenko, A. Johnson, F. W. Jones, J. Kallenbach, N. Kanaya, M. Kawabata, Y. Kawabata, M. Kawagut, S. Kelner, P. Kent, A. Kimura, T. Kodama, R. Kokoulin, M. Kossov, H. Kurashige, E. Lamanna, T. LampAcn, V. Lara, V. Lefebure, F. Lei, M. Liendl, W. Lockman, F. Longo, S. Magni, M. Maire, E. Medernach, K. Minamimoto, P. Mora de Freitas, Y. Morita, K. Murakami, M. Nagamatu, R. Nartallo, P. Nieminen, T. Nishimura, K. Ohtsubo, M. Okamura, S. O'Neale, Y. Oohata, K. Paech, J. Perl, A. Pfeiffer, M. G. Pia, F. Ranjard, A. Rybin, S. Sadilov, E. Di Salvo, G. Santin, T. Sasaki, N. Savvas, Y. Sawada, S. Scherer, S. Sei, V. Sirotenko, D. Smith, N. Starkov, H. Stoecker, J. Sulkimo, M. Takahata, S. Tanaka, E. Tcherniaev, E. Safai Tehrani, M. Tropeano, P. Truscott, H. Uno, L. Urban, P. Urban, M. Verderi, A. Walkden, W. Wander, H. Weber, J. P. Wellisch, T. Wenaus, D. C. Williams, D. Wright, T. Yamada, H. Yoshida, and D. Zschiesche, "Geant4-a simulation toolkit," Nucl. Instrum. Methods Phys. Res. A **506**, 250–303 (2003).
[12]R. Brun and F. Rademakers, "ROOT-an object oriented data analysis framework," Nucl. Instrum. Methods Phys. Res. A **389**, 81–86 (1997).
[13]I. Buvat and I. Castigilioni, "Monte Carlo simulations in PET and SPECT," Q. J. Nucl. Med. **46**, 48–61 (2002).
[14]G. Santin, D. Strul, D. Lazaro, L. Simon, M. Krieguer, M. Vieira Martins, V. Breton, and C. Morel, "GATE: A Geant4-based simulation platform for PET and SPECT integrating movement and time measurement," IEEE Trans. Nucl. Sci. **50**(5), 1516–1521, (2003).
[15]J. S. Karp, M. E. Daube-Witherspoon, E. J. Hoffman, T. K. Lewellen, J. M. Links, W-H. Wong, R. D. Hichwa, M. E. Casey, J. G. Colsher, R. E.

Hitchens, G. Muehllehner, and E. W. Stoub, "Performance standards in positron emission tomography," J. Nucl. Med. **32**, 2342–2350 (1991).
[16]"NEMA standards publication NU 2-1994: Performance measurements of positron emission tomographs," *Technical report* (National Electrical Manufactures Association, Washington, DC, 1994).
[17]"NEMA standards publication NU 2-2001: Performance measurements of positron emission tomographs," *Technical report* (National Electrical Manufactures Association, Washington, DC, 2001).
[18]K. Assié, V. Breton, I. Buvat, C. Comtat, S. Jan, M. Krieguer, D. Lazaro, C. Morel, M. Rey, G. Santin, L. Simon, D. Strul, J.-M. Vieira, and R. Van de Walle, "Monte Carlo simulation in PET and SPECT instrumentation using GATE," Nucl. Instrum. Methods Phys. Res. A **527**, 180–189 (2004).
[19]S. Jan, C. Comtat, D. Strul, G. Santin, and R. R. Trébossen, "Monte Carlo Simulation for the ECAT EXACT HR+ system using GATE," IEEE Trans. Nucl. Sci. (to be published).
[20]F. Lamare, A. Turzo, Y. Bizais, and D. Visvikis, "Simulation of the allegro PET system using GATE," Proc. SPIE **5368**, 890–897 (2004).
[21]S. Staelens, D. Strul, G. Santin, M. Koole, S. Vandenberghe, Y. D'Asseler, I. Lemahieu, and R. Van de Walle, "Monte Carlo simulations of a scintillation camera using GATE: Validation and application modeling," Phys. Med. Biol. **48**, 3021–3042 (2003).
[22]K. Assié, I. Gardin, P. Vera, and I. Buvat, "Validation of Monte Carlo simulations of Indium 111 SPECT using GATE," *Proc. of the 51th SNM Annual Meeting*, J. Nucl. Med. 45, 438 (2004).
[23]S. Jan, A. F. Chatziioannou, C. Comtat, D. Strul, G. Santin, and R. Trébossen, "Monte Carlo simulation for the microPET P4 system using GATE," Mol. Imag. Biol. **5**, 138 (2003).
[24]M. Rey, L. Simon, D. Strul, J-M. Vieira, and C. Morel, "Design study of the ClearPET LSO/LuYAP phoswich detector head using GATE," Mol. Imag. Biol. **5**, 119 (2003).
[25]D. Lazaro, I. Buvat, G. Loudos, D. Strul, G. Santin, N. Giokaris, D. Donnarieix, L. Maigne, V. Spanoudaki, S. Styliaris, S. Staelens, and V. Breton, "Validation of the GATE Monte Carlo simulation platform for modeling a CsI(Tl) scintillation camera dedicated to small-animal imaging," Phys. Med. Biol. **49**, 271–285 (2004).
[26]L. Simon, D. Strul, G. Santin, M. Krieguer, and C. Morel, "Simulations of time curves in small animal PET using GATE," Nucl. Instrum. Methods Phys. Res. A **527**, 190–194 (2004).
[27]F. Rannou, V. Kohli, D. Prout, and A. Chatziioannou, "Investigation of OPET performance using GATE, a Geant4-based simulation software," IEEE Trans. Nucl. Sci. **51**, 2713–2717 (2004).
[28]C. R. Schmidtlein, S. A. Nehmeh, L. M. Bidaut, Y. E. Erdi, J. L. Humm, H. I. Amols, and A. S. Kirov, "Validation of GATE Monte Carlo simulations for the GE Advance PET scanner," *Proc. of the 51th SNM Annual Meeting*, J. Nucl. Med. 45, 409–410 (2004).
[29]T. K. Lewellen, S. G. Kohlmyer, R. S. Miyaoka, S. F. Schubert, and C. W. Stearns, "Investigation of the count rate performance of the General Electric Advance positron emission tomograph," IEEE Trans. Nucl. Sci. **42**, 1051–1057 (1995).
[30]T. K. Lewellen, S. G. Kohlmyer, R. S. Miyaoka, M. S. Kaplan, C. W. Stearns, and S. F. Schubert, "Investigation of the performance of the General Electric Advance positron emission tomograph in 3D mode," IEEE Trans. Nucl. Sci. **43**(4), 2199–2206 (1996).
[31]J. F. Carrier, L. Archambault, and L. Beaulieu, "Validation of Geant4, an object-oriented Monte Carlo toolkit, for simulations in medical physics," Med. Phys. **31**, 484–492 (2004).
[32]D. E. Cullen, J. H. Hubbell, and L. Kissel, "EPDL97: The evaluated photon data library, 97 version," *Technical Report 5* (Lawrence Livermore National Laboratory, Los Alamos, NM, (1997).
[33]D. E. Cullen, S. T. Perkins, and S. M. Seltzer, "Tables and graphs of electron interaction cross 10 ev to 100 gev derived from the LLNL evaluated electron data library (EEDL), $z=1-100$," *Technical report* (Lawrence Livermore National Laboratory, Los Alamos, NM, 1991).
[34]S. T. Perkins, D. E. Cullen, M. H. Chen, J. H. Hubbell, J. Rathkopf, and J. Scofield, "Tables and graphs of atomic subshell and relaxation data derived from the LLNL evaluated atomic data library (EADL), $z=1-100$," *Technical report*, (Lawrence Livermore National Laboratory, Los Alamos, NM, 1991).
[35]OpenGATE Collaboration, *GATE Users Guide, Version 1.0.0*, May 2004, http://www-lphe.epfl.ch/GATE/
[36]L. Eriksson, K. Wienhard, and M. Dahlbom, "A simple loss model for positron camera systems," IEEE Trans. Nucl. Sci. **41**(4), 1566–1570 (1994).
[37]E. J. Hoffman, S-C. Huang, M. E. Phelps and D. E. Kuhl, "Quantitation in positron emission computed tomography: 4. Effect of accidental coincidences," J. of CT **5**(3), 391–400, (1981).
[38]R. Siegel and J. R. Howell, *Thermal Radiation Heat Transfer*, 4th ed. (Taylor and Francis-Hemisphere, Washington, 2001).
[39]G. F. Knoll, *Radiation Detection and Measurement*, 3rd ed. (Wiley, New York, 2000).
[40]M. E. Daube-Witherspoon, J. S. Karp, M. E. Casey, F. P. DiFillippo, H. Hines, G. Muehllehner, V. Simcic, C. W. Stearns, L-E. Adam, S. G. Kohlmyer, and V. Sossi, "PET performance measurements using the NEMA NU 2-2001 standard," J. Nucl. Med. **43**(10), 1398–1409 (2002).
[41]S. G. Kohlmyer, C. W. Stearns, P. E. Kinahan, and T. K. Lewellen, "NEMA NU2-2001 performance results for the GE Advance PET system," IEEE Trans. Nucl. Sci. 890–894 (2002).
[42]R. D. Badawi, S. G. Kohlmyer, R. L. Harrison, S. D. Vannoy, and T. K. Lewellen, "The effect of camera geometry on singles flux, scatter fraction and trues and randoms sensitivity for cylindrical 3d pet—A simulation study," IEEE Trans. Nucl. Sci. **47**(3), 1228–1232 (2000).
[43]R. L. Harrison, S. D. Vannoy, D. R. Haynor, S. B. Gillispie, M. S. Kaplan, and T. K. Lewellen, "Preliminary experience with the photon history generator module of a public domain simulation system for emission tomography," in *Proc. IEEE Medical Imaging Conference*, San Francisco, CA, pp. 1154–1158.
[44]K. Thielemans, D. Sauge, C. Labbé, C. Morel, M. Jacobson, and A. Zverovich, *STIR Software for Tomographic Image Reconstruction: User's Guide, Version 1.3* Hammersmith Imanet, 2004, http://stir/irsl.org/documaentation/STIR-UsersGuid.pdf
[45]E. J. Hoffman, T. M. Guerrero, G. Germano, W. M. Digby, and M. Dahlbom, "Pet system calibrations and corrections for quantitative and spacially accurate images," IEEE Trans. Nucl. Sci. **36**(1), 1108–1112 (1989).
[46]B. Bendriem and D. W. Townsend, editors, "The Theory and Practice of 3D PET," vol. 32 of *Developments in Nuclear Medicine* (Kluwer Academic, Dordrecht, 1998).